

Extraction and localization of mesoscopic motor control signals for human ECoG neuroprosthetics

Justin C. Sanchez^{a,*}, Aysegul Gunduz^b, Paul R. Carney^a, Jose C. Principe^b

^a Neuroprosthetics Research Group, Department of Pediatrics, Division of Neurology, University of Florida, Gainesville, FL 32610, USA

^b Computational NeuroEngineering Laboratory, Department of Electrical and Computer Engineering, University of Florida, Gainesville, FL 32611, USA

Received 1 January 2007; received in revised form 26 April 2007; accepted 26 April 2007

Abstract

Electrocorticogram (ECoG) recordings for neuroprosthetics provide a mesoscopic level of abstraction of brain function between microwire single neuron recordings and the electroencephalogram (EEG). Single-trial ECoG neural interfaces require appropriate feature extraction and signal processing methods to identify and model in real-time signatures of motor events in spontaneous brain activity. Here, we develop the clinical experimental paradigm and analysis tools to record broadband (1 Hz to 6 kHz) ECoG from patients participating in a reaching and pointing task. Motivated by the significant role of amplitude modulated rate coding in extracellular spike based brain–machine interfaces (BMIs), we develop methods to quantify spatio-temporal intermittent increased ECoG voltages to determine if they provide viable control inputs for ECoG neural interfaces. This study seeks to explore preprocessing modalities that emphasize amplitude modulation across frequencies and channels in the ECoG above the level of noisy background fluctuations in order to derive the commands for complex, continuous control tasks. Preliminary experiments show that it is possible to derive online predictive models and spatially localize the generation of commands in the cortex for motor tasks using amplitude modulated ECoG.

© 2007 Elsevier B.V. All rights reserved.

Keywords: Electrocorticogram; ECoG; Brain–machine interface; Brain–computer interface; Human motor control; Feature extraction; Localization; Cortex; Neuroprosthetic

1. Introduction

Recent advances in motor neuroprosthetic experimental designs will likely offer new rehabilitation options to patients who have lost their ability to move due to disease or injury to the central or peripheral nervous system. The great potential for direct neural interfaces to aid the disabled has been demonstrated through the control of computer cursors, prosthetic limbs, and functional electrical stimulation systems (Scott, 2006; Editorial, 2006).

From a methodological perspective, spatial scale has played an important role in brain–machine interface (BMI) develop-

ment and includes the use of spikes (action potentials – local to the neuron) (Sanchez et al., 2003a,b; Serruya et al., 2002; Taylor et al., 2002; Wessberg et al., 2000; Nicolelis, 1999), local field potentials (Rickert et al., 2005a,b), electrocorticogram (ECoG) (Leuthardt et al., 2004), and electroencephalogram (EEG) (Pfurtscheller and da Silva, 1999; Wolpaw et al., 2002). Harnessing a sufficient representation from both the inputs (dendritic activity) and outputs (action potentials) of neural assemblies seems to be critical for interpreting the intent of the individual. The evidence for BMI control using spontaneous ECoG activity is limited and may not be as direct as micro-electrode recordings (Leuthardt et al., 2006; Sanchez et al., 2006), but partial information of natural intent of movement exists when the spontaneous ECoG is time locked averaged to the stimulus (Leuthardt et al., 2004; Mehring et al., 2004). Several groups have laid a foundation for demonstrating that ECoG contains information related to motor tasks both in monkeys and humans. Of these groups, researchers have begun using ECoG recordings from human patients in epilepsy studies and have successfully demonstrated a motor neuroprosthetic for directional

Abbreviations: ECoG, electrocorticogram; EEG, electroencephalogram; BMI, brain–machine interface; BCI, brain–computer interface; P, posterior parietal cortex; M1, primary motor cortex; PM, premotor cortex; S, somatosensory cortex

* Corresponding author at: University of Florida, P.O. Box 100296, JHMHSC Gainesville, FL 32610, USA. Tel.: +1 352 846 2180; fax: +1 352 392 9802.

E-mail address: jcs77@ufl.edu (J.C. Sanchez).

cursor control tasks using frequency analysis (Leuthardt et al., 2004). Leuthardt and colleagues (Leuthardt et al., 2004; Wolpaw et al., 2002; McFarland et al., 1997; Vaughan and Wolpaw, 2006; Schalk et al., 2004; Leuthardt et al., 2003) found that ECoG signals derived through spectral analysis were associated with motor and speech imagery and patients could achieve success rates of 74–100% in a one-dimensional binary task. In other work, the relative information in sensorimotor rhythms, slow cortical potentials, and P300 evoked potentials have been compared for use in motor control using autoregressive modeling (Leuthardt et al., 2006; Leuthardt et al., 2003; Heldman et al., 2006). Aertsen and colleagues have used information theoretic approaches for extracting motor commands and compared the results to directional tuning (Mehring et al., 2003a,b; Riehle et al., 1997; Wennekers et al., 2003; Aertsen et al., 2003; Rickert et al., 2005a,b). These results demonstrate the proof-of-concept that ECoG can provide viable control signals for rehabilitative neuroprosthetics. The main methodology employed in current ECoG BMIs is analysis of event related potentials (ERP) (Makeig, 1993; Lutzenberger et al., 1992; Johnson et al., 1977). ERP methods focus on extracting binary classification features for the studied stimuli which are each used in controlling a dimension of neuroprosthetic movement. While the use of ERPs have been shown for cursor control, the instantaneous tracking of continuous movement trajectories could benefit from additional information contained in the ECoG. The hypothesis of this paper is that there is an increased frequency dependent spatial neuromodulation correlated with movement that can be extracted from the spontaneous ECoG. The next obvious step for testing this realization of an ECoG BMI is therefore to develop and validate new experimental paradigms and signal processing methodologies for real-time neural prosthetics (Andersen et al., 2004).

A natural question that will be pursued in this paper is to find out if one can obtain descriptors of movement intent directly from ECoG activity that leverages concepts used in microscopic approaches. With this we mean to develop online signal processing algorithms that extract real-time signatures from the spontaneous neuromodulation activity. Unfortunately, very little is known about what spatio-temporal information is accessible in the spontaneous background activity, which normally is referred as “EEG/ECoG noise”. In order to investigate this question, two fundamental requirements seem necessary: experimentation with cooperative subjects to obtain feedback and signal processing methodologies that can find descriptors that modulate with the motor behavior. In this work, we develop an experimental paradigm and analysis tools to use the electrocorticogram (ECoG) in a motor control experimental paradigm that can provide a means of communication for paralyzed patients. Since it is well known that amplitude modulation plays a key role in both neuronal activation and rate coding, seeking spatial pattern classification and temporally intermittent population synchronization/depolarization may be a good starting choice. This study seeks to explore preprocessing modalities that emphasize ECoG amplitude modulation above the noise level and background fluctuations in order to derive the commands for complex motor control tasks (reaching and grasping). We propose to use

simultaneous feature detection and model optimization to guide the selection of neural potentials that modulate in response to motor tasks. High resolution signal analysis (12 kHz sampling) with human ECoG electrode arrays will provide the experimental paradigm and broadband spectra to derive amplitude modulations for learning the relationship between the generation of ECoG potentials and hand/arm movement. We will present techniques to spatially localize the potentials most related to the behavioral tasks and compare them with traditional techniques used for analyzing ECoG.

2. Materials and methods

2.1. Preliminary studies

The success of ECoG BMIs relies heavily upon the ability to extract features from neural activity related to goal directed behavior. Theoretical analyses outlined by Freeman (Freeman, 1975; Freeman, 2000; Freeman, 2004a; Freeman, 2004b; Freeman, 2005; Freeman, 2006) and Nunez (Nunez, 1981; Nunez, 1989; Nunez, 1995) have identified the utility of ECoG potentials and attempts to explain how to extract the relevant modulation of neural assemblies. Closely spaced subdural electrodes have been reported to measure the spatially averaged bioelectrical activity of an area much smaller than several square centimeters (Pfurtscheller et al., 2003). The production of potentials is due to the superposition of many aligned and synchronous dipole sources (Nunez, 1981). The coactivation of sources is related to neural “synchrony” and is used to describe the amplitude modulations in extracellular recordings that occur during state changes (Pfurtscheller and da Silva, 1999). The fluctuating cortical potentials have been associated with traveling waves of local dendritic and axonal potentials (Thatcher et al., 1986). The results in (Thatcher et al., 1986) indicate that at least two separate sources of signal coherence are produced either through the action of short length axonal connections or the action of long distance connections. Synchronous activity can occur at different spatial scales and over time lags (Nunez, 1981) which requires wide spatial sampling of the cortex and analysis over fine temporal scales. The ability to detect and localize the mesoscopic neuronal activation (cumulative sum of EPSPs/IPSPs and action potentials across the ensemble) from ECoG electrodes is dependent upon an empirical inverse power relation (log power decreases by “ $1/f^b$ ”, $b \sim 2 \pm 1$) (Freeman and van Dijk, 1987; Barrie et al., 1996). The biophysical attenuation properties of the neural media make the detection of fast, amplitude modulation (<1 ms) in ionic concentration difficult to detect. The power spectrum of an extracellular potential depends upon the size of the cortical column (or dipole layer) sampled. The size of the activated column should be proportional to the spatial scale of the recording electrode to minimize the dynamic functional relationships between the observed power spectrum and that of the tissue itself (Nunez, 1981). For ECoG, it is estimated that 10^5 neurons are contributing to the extracellular potential variations (Abeles, 1982).

The origin of the state of electrophysiological oscillations among neurons likely depends on the density of negative feed-

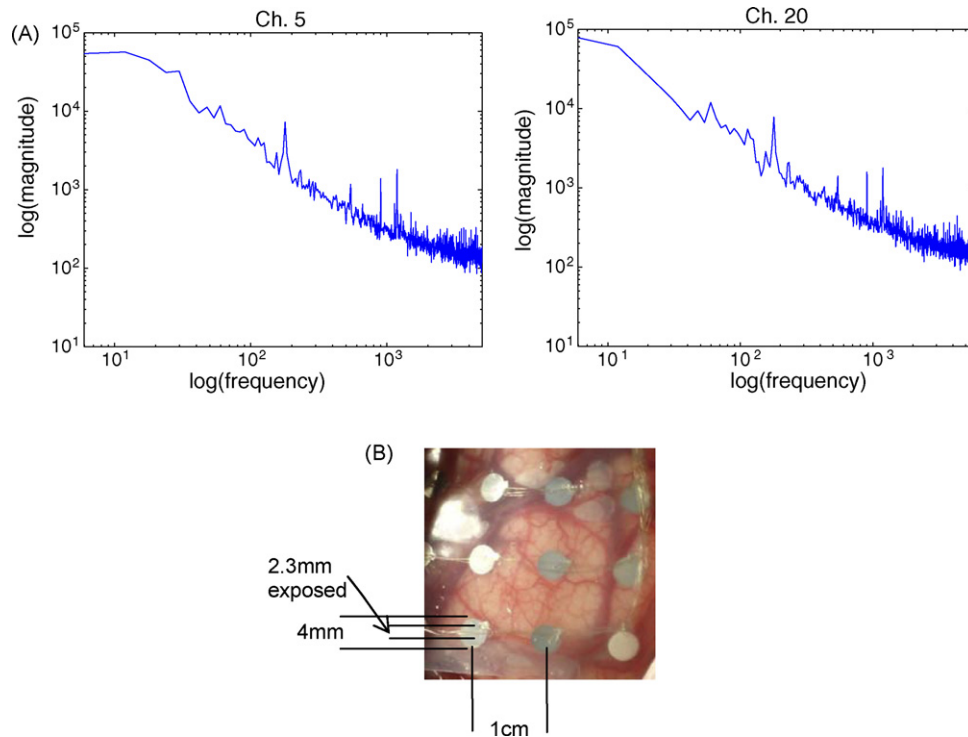


Fig. 1. (A) Spectra of human ECoG recordings from this study averaged over 10 windows 10 s in length. Plotted in log–log coordinates, the data demonstrates a $1/f$ trend. (B) *In vivo* placement of the electrode grid in a 3 cm \times 3 cm area of cortex and the relative electrode, gyri, sulci, and vasculature relationships.

back connections between excitatory and inhibitory nodes, the ratio of short to long connections, and the magnitude of the background noise. Here understanding the role of noise is critical for accurately extracting the oscillations among neurons. To elucidate this relationship, we present in Fig. 1A the power spectra¹ (PSD) for real human ECoG recordings (details will be described in the next section) in log–log coordinates. Here, the slope of the curve indicates the well-known power–law relationship of scale free networks and is very telling of the relationships between intentional oscillations and noise (Freeman, 2005; Freeman, 2006). The slope of the PSD in subjects at rest is known to range between $\alpha = -2$ and -3 . In this case, the patient was engaged in a behavioral task where arousal brings peaks above the linear slope of -1 to -2 . The significance of the unique spectral peaks as well as the decreasing slope at frequencies above 3 kHz is difficult to assess from spectral analysis alone and hence motivates the use of behavioral experiments in the following sections.

2.2. Patients

The subjects participating in the neuroprosthetic study were undergoing extraoperative subdural grid evaluation for the treatment of intractable complex partial epilepsy at Shands Hospital at the University of Florida. Both patients involved in the study were right-handed females. Patient 1 was 14 years old while Patient 2 was 15 years old. All experimental protocols were

approved by the University of Florida IRB. Prior to ECoG subdural electrode implantation, both patients underwent a presurgical work-up that included scalp EEG, formal neuropsychological testing, and MRI. The patients' motor capacities were verified to be in a normal range as verified through neuropsychological testing. In addition, motor functions were verified to be nonfocal by the absence of motor or sensory deficits on neurological examination. It is important to note here that while epileptic patients presented with intact motor functions, the disease can influence brain function for BMI studies designed in this manner as has been discussed in other studies (Leuthardt et al., 2004; Mehring et al., 2004).

As a part of the standard of care, the patients were implanted with subdural grid electrodes. The surgical implantation of the electrode grids was performed according to established protocols (Lesser et al., 1990) and the grids consisted of a 1.5 mm thick silastic sheet embedded with platinum–iridium electrodes (4 mm diameter with 2.3 mm diameter exposed surface) spaced at 1-cm center-to-center distances. A picture of the implanted grid on a 3 cm \times 3 cm surface of cortex is presented in Fig. 1B. Here, we can observe the size relationships between the effective electrode diameter, spacing, and orientation with respect to gyri, sulci, and vasculature both on the cortex and in the sulci. The approximate electrode position and numbering as indicated by the surgeon at the time of surgery is presented in Fig. 2A for Patient 1 and 2B for Patient 2. The location of the electrode grids was also evaluated using MRI (1.5 T) under the guidance of a board certified radiologist. In Fig. 2C and D, the post-operative T1 weighted images are shown for each of the patients in this study. The method of defining the anatomical location of the

¹ The FFT was computed with 2048 points and was averaged over 10 windows of 10 s in duration.

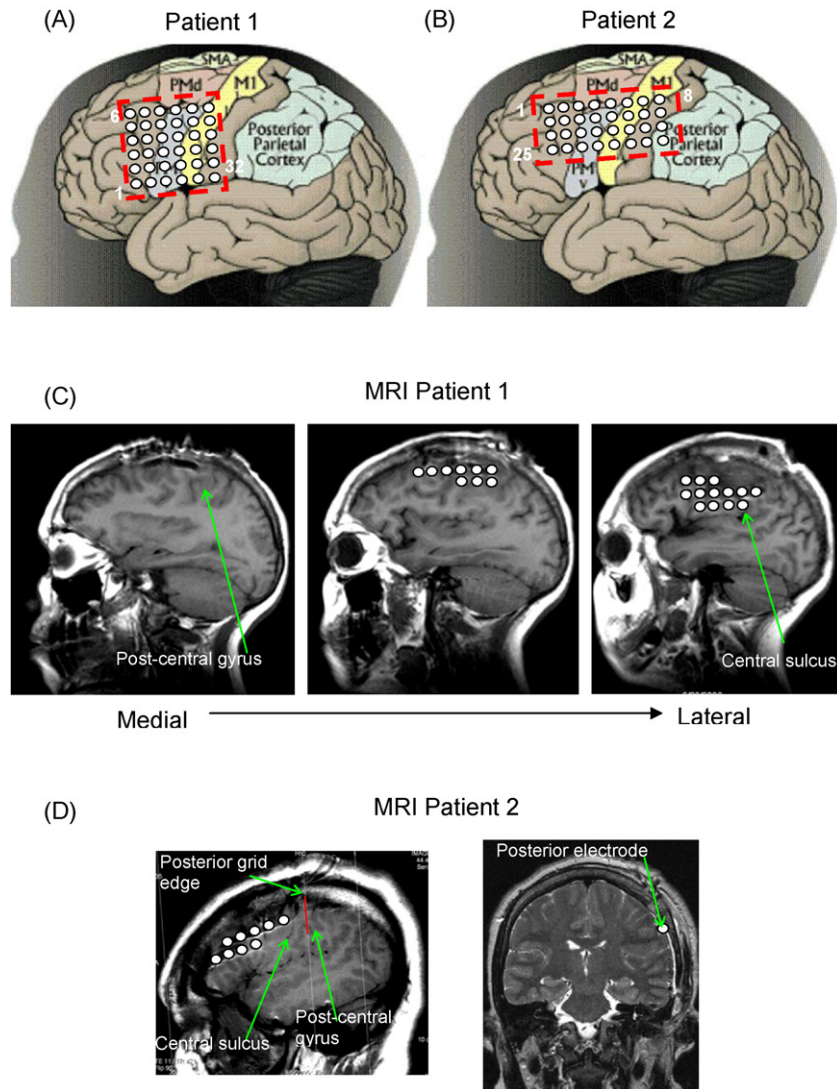


Fig. 2. Summary of the grid localization. (A and B) Electrode placement and numbering for Patient 1 and Patient 2 as indicated by the surgeon. (C and D) Anatomical localization of grid electrodes via T1 MR imaging. Under the guidance of a board certified radiologist, the location of the grid electrodes was determined by identification of anatomical landmarks such as the pre-central and post-central gyri and the central sulcus.

grid consisted of first identifying the post-central gyrus working from the midline and then following it to the central sulcus. With these landmarks, the grid electrodes were identified and labeled in the images and markers were applied. The relative positions of the electrodes with respect to the central sulcus and surrounding gyri allowed association of the electrodes with either premotor (PM), primary motor (M1), somatosensory (S), and posterior parietal (PP) cortices. We would like to note here that due to the clinical imaging protocol the slice thickness is large (5 mm thickness and a skip of 2.5 mm) and did not always provide the best imaging orientation (as with Patient 2) for localization. Therefore, multiple images were required to completely localize the grid with respect to the central sulcus as shown by the partial labeling of the grid in each image.

The patients involved in this study were fully recovered from the grid electrode implantation surgery within 48 h post-surgery and were fully alert and attentive at the time of testing.

During their epilepsy work-up, the patients were tapered from their presurgical anticonvulsant medications (topiramate, oxcarbazepine) to facilitate seizure evaluation. When the behavioral tasks were performed, the patients were seizure free for at least 6 h prior to testing. The location of the primary motor cortex was also determined by evoked potentials and direct electrical stimulation of the subdural grids. The well-known stimulation paradigm (Jasper and Penfield, 1954) consisted of biphasic waves with pulse duration 0.3 ms, a pulse train of 2–5 s, at a rate 50 Hz. The stimulus intensity began at 2 mA and increased by 1 or 2 mA increments. Motor responses from the stimulation, using the numbering convention in Fig. 2A and B, for Patient 1 were derived from electrodes (22, 28 – wrist), (23, 24, 30 – hand), (22, 30 – forearm), (29 – bicep), (27 – sensory arm), while Patient 2 responded with electrodes (2, 3 – hand), (14, 15 – arm). For the purposes of this study, the seizure focus for each patient was determined to be far from the motor region of interest.

2.3. Behavioral task

The behavioral task used in this neuroprosthetic design is focused on arm reaching and pointing. For paralyzed patients, reaching and pointing offers two critical functions of the motor system: reaching enables one to extend the ranges of goals available while pointing enables one to communicate which goal is of interest (Shadmehr and Wise, 2005). This behavior for communication and control places emphasis on the neural decision making process that controls the motor exploration of a patient's environment and the visual feedback of the resulting movements. The visuomotor behavior presented here will require motor commands that orient a patient's arm and locomotion toward a visual input. This behavior is also known as a standard sensorimotor approach mapping (Wise et al., 1996). In this first step in extracting ECoG commands for neuroprosthetics, the standard sensorimotor approach provides a simple basis of investigation compared to more complicated transformational or guess-guided movements. To execute and acquire the behavior described here, the patients were cued to follow with their index finger a predefined cursor trajectory presented on an LCD screen with an active area of (20 cm × 30 cm). The trajectory in Fig. 3 consisted of two components: a commonly used center-out cursor control task (Georgopoulos et al., 1982) and a target selection (Desmurget et al., 1998) task. The center-out task consisted of smoothly varying trajectories that formed a pattern extending from the center to predefined locations (invisible to the patient) at the edges of the work area. For the target selection task, color-coded targets are arranged in a sequence at the top of the screen and the patient was required to move to each of them. This behavior mimics a computer user's movement to select an icon on the screen. In a single session, the patients were required to repeat the entire task six times. In the center-out task, the cursor moves from the center of the screen to each of the corners and mid-sides as shown in Fig. 3 (actual trajectory). This is immediately followed by the target selection in which the cursor reaches to each of the five horizontally aligned targets once and returns to its initial position in between targets. This entire trajectory was repeated for each trial. For the patients presented here, Patient 1 was able to complete the tasks at a speed that was 15% faster Patient 2. All behavioral tasks were acquired concurrently with the recording of neuronal modulations from the implanted ECoG grids.

2.4. Recording methodology

The extraction of communication and control features from ECoG within a brain-machine interface (BMI) paradigm is facilitated by the ability to continuously time synchronize neuronal modulation with known variables in the external environment. Here, the experimenter can gain an advantage by directly correlating internal neural representations with well defined behavioral tasks. However, the well controlled experimental paradigms that monitor and synchronize neural activity with behavior in the laboratory are difficult to replicate in the clinical environment. The first priority is always patient care; therefore, all monitoring equipment is tailored for clinical evaluation,

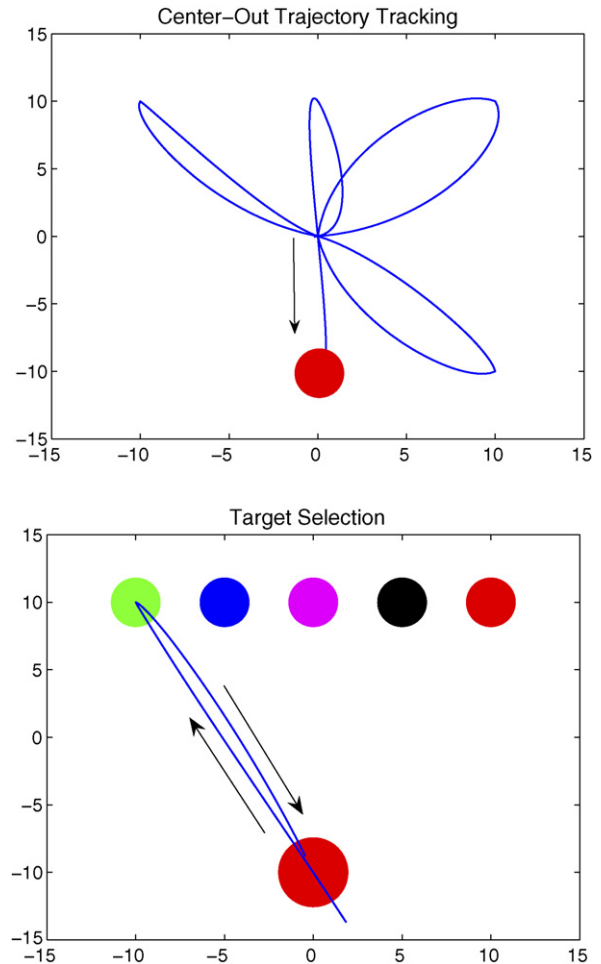


Fig. 3. Behavioral trajectories which consisted of a center-out reaching task and a target selection task (pointing) in 20 cm × 30 cm work area (x – horiz., y – vert.). The patients were cued to follow with their index finger a predefined cursor trajectory presented on an LCD screen. The trajectory consisted of two components: a commonly used center-out cursor control task and a target selection task. The targets are arranged in a sequence at the top of the screen.

in this case, of epilepsy which may not be suited to evaluate the host of available control signals that can be extracted from ECoG. Moreover, in addition to the standard electrophysiological equipment, a variety of other monitoring devices (pulse oximeter, etc.) can contribute noise sources.

To overcome these challenges of the clinical environment, we designed a recording paradigm shown in Fig. 4 that augments the clinical monitoring systems during the duration of the experiments presented here with larger bandwidth amplifiers, but from which the conventional ECoG can be recovered with the same clinical quality. The choice of a broader bandwidth was motivated by theoretical studies of biophysical limits of frequency resolution which implies that potentials up to 10 kHz are observable in ECoG (Nunez, 1981). Working from left to right in the diagram, a custom cable was designed to interface the clinical Ad-Tech (Racine, Wisconsin) electrodes with the biopotential amplifiers. To minimize noise contamination encountered in the clinical environment, the amplifiers were placed close to the patients head by minimizing the custom cable length. Next, the amplified and digitized neuronal activity is sent optically to a

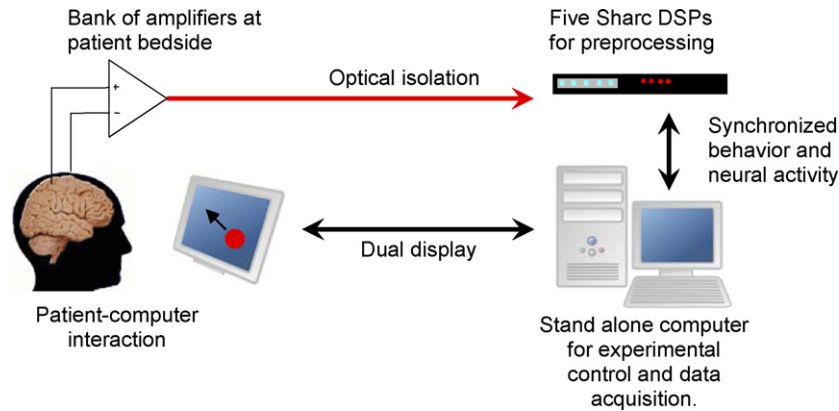


Fig. 4. Schematic of the recording methodology. The goal is to simultaneously record ECoG potentials (up to the biophysical limit of frequency resolution) and behavior. Working from left to right, a custom cable was designed to interface the clinical Ad-Tech electrodes with the biopotential amplifiers. To minimize noise encountered in the clinical environment, the amplifiers were placed close to the patients head. Next the amplified and digitized neuronal activity is sent optically to a bank of DSPs that preprocess (filter) the data. The data is then sent via a gigabit PCI interface to the recording computer which was generating the desired behavior through a Matlab ActiveX interface. Finally, the desired trajectories were sent to a second computer monitor placed in front of the patient.

bank of DSPs that preprocess (filter) the data and time synchronize it with the behavioral trajectories. In the multi-DSP architecture, each DSP could be assigned a particular task to distribute the processing. A desktop computer (Dell XPS, Pentium 4, 3 GHz, 2 GB RAM, 1 TB Hard disk, RAID 5 configuration) running Matlab v7 was generating the desired behavioral trajectories and communicating with the bank of DSPs through ActiveX commands. The data was then sent via a bi-directional gigabit PCI interface between the recording computer which was storing data and generating the desired behavior while communicating with the DSPs. Finally, the desired trajectories were sent to a second computer monitor placed in front of the patient. The patient was then cued to follow the cursor trajectory with their index finger. During the task, the recordings were supported by a full clinical staff including a board certified neurologist and the technicians of Shands Hospital Epilepsy Monitoring Unit. This step ensures that the qualified personnel are present to monitor the patient during the study in compliance with the “standard of care” of epilepsy practice. The clinical epilepsy monitoring team had full access to the ECoG monitoring system in conjunction with video surveillance to ensure patient safety.

2.5. Electrophysiological data collection

Multichannel subdural potentials were collected synchronously while the patients were engaged in the behavioral task. Neuronal activity from the electrodes indicated by the dashed boxes in Fig. 2A and B were recorded using a Tucker-Davis (Alachua, Florida) Pentusa neural recording system sampling at 12,207 Hz which is half of the native DSP clock, 24,414. 1 Hz. The neural recording system used in this study is capable of recording from 32 electrodes simultaneously. The sampling rate was determined using information from the preliminary studies which describes the biophysical limits of subdural neural recording. The potentials from the sampled cortical areas were digitized with 16 bits of resolution and bandpass filtered from 1 to 6 kHz which represents the Nyquist frequency. Behavioral trajectory recordings were also stored with a shared

time clock and sampled at 381.5 Hz on the Pentusa system using ActiveX controls described in 3.1.3 which were also sent to the patient display system shown in Fig. 4.

Representative recordings from the neuroprosthetic experimental paradigm are presented in Fig. 5. Time-synchronized ECoG and behavioral recordings from Patient 1 are plotted over a 5 s duration. The first subplot contains a segment of the center-out trajectory in (x, y) coordinates where the center of the screen is located at $(0, 0)$ and the excursions range from ± 20 cm in displacement. Subplots two and four present the raw time-series with broadband filtering (1 Hz to 6 kHz) recorded from the ECoG grid electrodes. Voltages in the range of $\pm 100 \mu\text{V}$ were observed. Combinations of low-amplitude fast oscillations were mixed with large amplitude slow and sharp waves. In subplots three and five, we present the spectrograms that correspond to the raw voltage traces. To compute the spectrogram, the raw ECoG recordings were windowed (Hamming) into segments of 512 points with 50% overlap. Here, the temperature of the colors (black maximum) corresponds to the FFT magnitude at each frequency. To maximize the ability to resolve the peaks of the spectra over the broad frequency range, the plot has been brightened and limited from 1 Hz to 4 kHz which contained the majority of the energy. We observe a $1/f$ decrease in the magnitude as the frequency is increased shown by the largest values of red at the lower frequency. A second feature that can be extracted from the spectrograms are the black vertical stripes that span the spectrum intermittently. Some of these are related to the sharp waveform features occurring spontaneously in the ECoG, while others occur synchronously with small amplitude modulations in the raw traces. A third feature is the horizontal stripes noted in the record at 12 kHz which corresponds to a harmonic of 60 Hz noise artifact. To summarize, from the spectrograms of this short segment of data the majority of the spectral energy is indeed at lower frequencies (i.e. < 500 Hz) however we also observe other high frequency modulations that span up to 4 kHz. Beyond 4 kHz, the appearance of spectral modulations was rare. The modulations up to 4 kHz were observed in both patients.

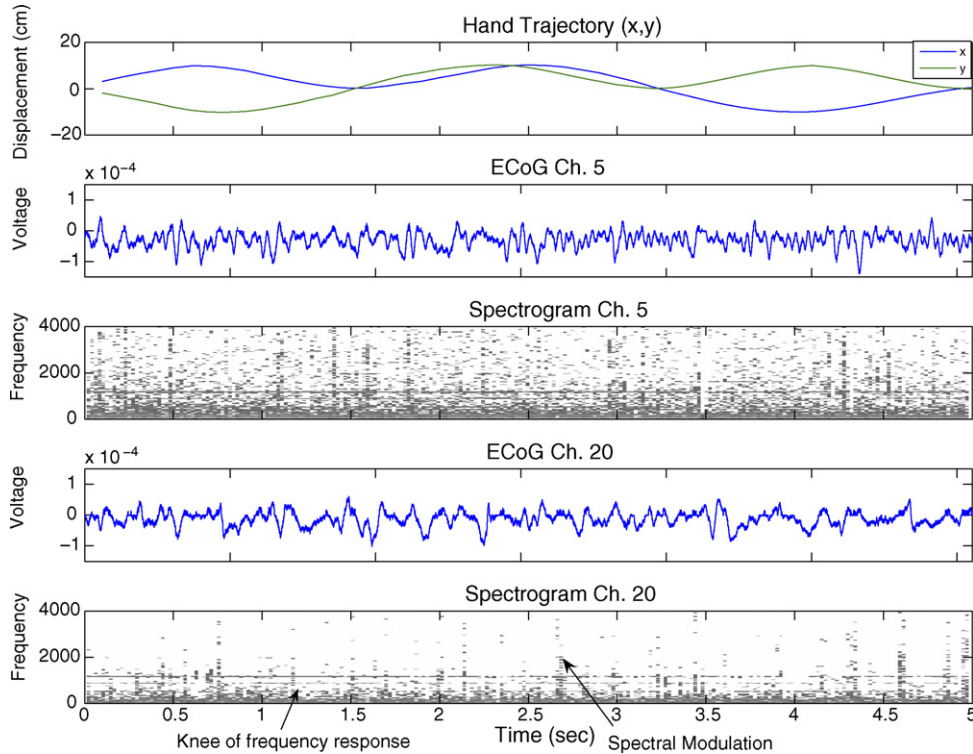


Fig. 5. Synchronized ECoG and behavioral recordings from Patient 1 over a 5 s duration. The first subplot contains a segment of the center-out trajectory in x, y coordinates where the center of the screen is located at $(0, 0)$ and the excursions range from ± 20 cm in displacement. Subplots two and four present the raw time-series with broadband filtering (1 Hz to 6 kHz) recorded from the ECoG grid electrodes. Voltages in the range of $\pm 100 \mu\text{V}$ were observed. In subplots three and five, we present the spectrograms that correspond to the raw voltage traces. Here, the temperature of the colors corresponds to the magnitude of the frequency response. Black signifies the largest magnitude.

2.6. Feature detection and extraction of control signals

2.6.1. Energy preprocessing and filtering

Sensorimotor ECoG rhythms have been studied extensively for assessing cortical activation for both theoretical and empirical reasons. The dynamic representations of information in distributed cortical neuronal networks have been shown to correlate with a variety of visual, auditory, and motor tasks and comprise the slow potentials and their sub-bands (1–60 Hz) (Pfurtscheller et al., 2003), gamma band (60–100 Hz) (Engel and Singer, 2001), fast gamma band (100–300 Hz) (Sinai et al., 2005) and ensemble depolarization (300–6 kHz) as coined in (Engel et al., 2005). One of the challenges of processing ECoG sensorimotor rhythms is that it is difficult to extract the relevant information over the noise. An approach to overcoming the temporal averaging of trials is to build upon the strengths of rate coding preprocessing that has been used extensively in single-trial, single-unit BMI experiments (Sanchez et al., 2003a,b). The critical advantage of rate coding approaches is that timing information in neuronal firing is translated into amplitude information as represented in bin rates (# of spikes per unit time). Typical firing rates are computed in bins of 100 ms (Sanchez et al., 2003a,b). The goal here is to employ a similar method of preprocessing in ECoG recording where sensorimotor amplitude modulations within specific bands are converted into “rate-like” information. However, in the case of ECoG the signals of interest are less specific since the measured signals are the coactivation

of many neural sources spread within a volume of the cortex. Since the specific relationships between instantaneous amplitude modulations are still largely unknown, we opt to first select broadband filtering to reduce the influence of strong assumptions. In this study, we seek amplitude modulations within the broad categories of modulations defined in the literature consisting the slow (1–60 Hz), gamma (60–100 Hz), fast gamma (100–300 Hz), and ensemble (300 Hz to 6 kHz) to determine how instantaneous amplitude modulations in each contribute hand reaching and pointing. Therefore, we define the band specific amplitude modulation as the sum of the power of the ECoG (Worrell et al., 2002) voltage signal in a 100 ms time bin as in Eq. (1).

$$x(t_n) = \sum_{i=1}^{100 \text{ ms}} v^2(t_n + i), \quad \text{where } t_{n+1} = t_n + 100 \text{ ms.} \quad (1)$$

In this paradigm we equally weight positive and negative polarizations and focus only on the power. Eq. (1) was computed in 100 ms non-overlapping windows for each electrode over the entire dataset in each of the bands that were pre-processed using equiripple FIR filters adjusted for the group delay. Representative traces of the filtered amplitude modulations (AM) time synchronized with behavior are presented in Fig. 6. The amplitude modulations separated into four frequency bands decrease in magnitude with increasing frequency (2 orders from 60 to 100 Hz and 1 order from 300 to 6 kHz). Qualitatively,

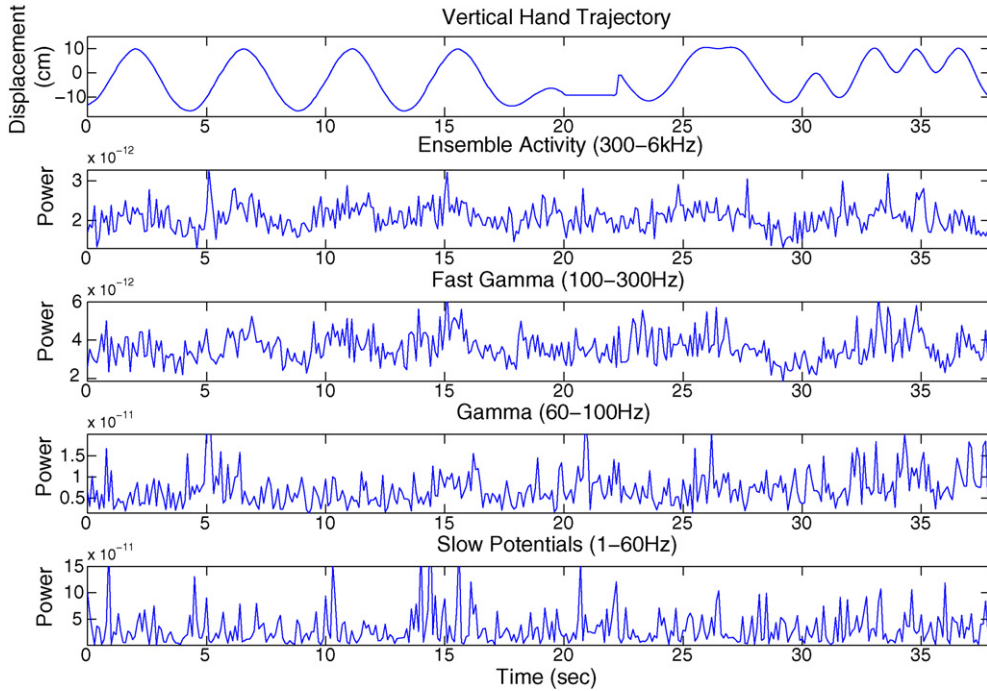


Fig. 6. Preprocessing of the raw voltage ECoG recordings via Eq. (2) yielded the traces in subplots 2–5. The amplitude modulations are separated into four frequency bands. Qualitatively, the correlation of the AM patterns with the behavior were observed to increase with the frequency as shown in the higher frequency bands (100–300 Hz, 300–6 kHz).

the integrated amplitude modulations of the higher frequencies (100–300 Hz, 300–6 kHz) produce waveforms (non-zero) that correlate well with the desired signal when viewed over a time span of 5 s. These waveforms are smoother than the lower frequencies (1–100 Hz) which produce spiky waveforms that deviate from zero.

2.6.2. Modeling

Now that the fundamental properties of the experimental paradigm and the raw ECoG have been characterized, we will address the extraction of control features from the preprocessed AM data on a single-trial basis. The methodology to achieve such a goal is to adapt a linear (or nonlinear (Sanchez et al., 2002)) model to the data during the trials, where the input is the multi-channel amplitude modulated ECoG, and the desired response is the motor control task. Effectively, we are doing identification of the system that transforms in real time the ECoG signals to movement. The advantage of this technique is that it does not require averaging, and the trained model is capable of controlling directly the interface. The disadvantage is that it is still a “black box” model in the sense that without further analysis we do not know what features are relevant; however we will explore the implications of the features in the next section.

To construct the mapping between AM ECoG neuronal modulation and behavior, a linear adaptive finite impulse response (FIR) filter topology in Fig. 7 was trained using the Wiener solution (Haykin, 1996). The topology contains 32 inputs (ECoG channels), 25 tap-delays (optimized to find the best generalization), and two outputs and was trained with 4 min (2400 samples) of ECoG and behavioral recordings. The Wiener filter utilizes

the most recent 2.5 s of neural activity to compute each output which was optimized by scanning tap-delays from 5 to 30 to construct the best performance. The inputs and desired signals used for this topology were normalized to zero mean and unit variance. The vector form of this operation is given by (2) (Sanchez et al., 2003a,b). The optimal MSE solution is given by (3), where d is the hand trajectory. The testing output trajectories (generated on 1.5 min of novel data) of the trained model using the Wiener solution are presented in Fig. 8. Here, a separate model is created for each frequency band. The trajectories are presented for both x (horizontal) and y (vertical) position and velocity.

$$\mathbf{y}(t) = \mathbf{W}\mathbf{x}(t) \quad (2)$$

$$\mathbf{W} = \mathbf{R}^{-1}\mathbf{P} = E(\mathbf{x}^T\mathbf{x})^{-1}E(\mathbf{x}^T\mathbf{d}) \quad (3)$$

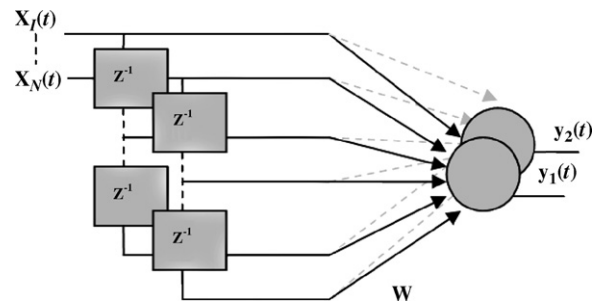


Fig. 7. Finite impulse response (FIR) filter topology. Here, the variable x refers to the preprocessed neural inputs while $y_1(t)$ and $y_2(t)$ represent the horizontal and vertical axes of the movement trajectory.

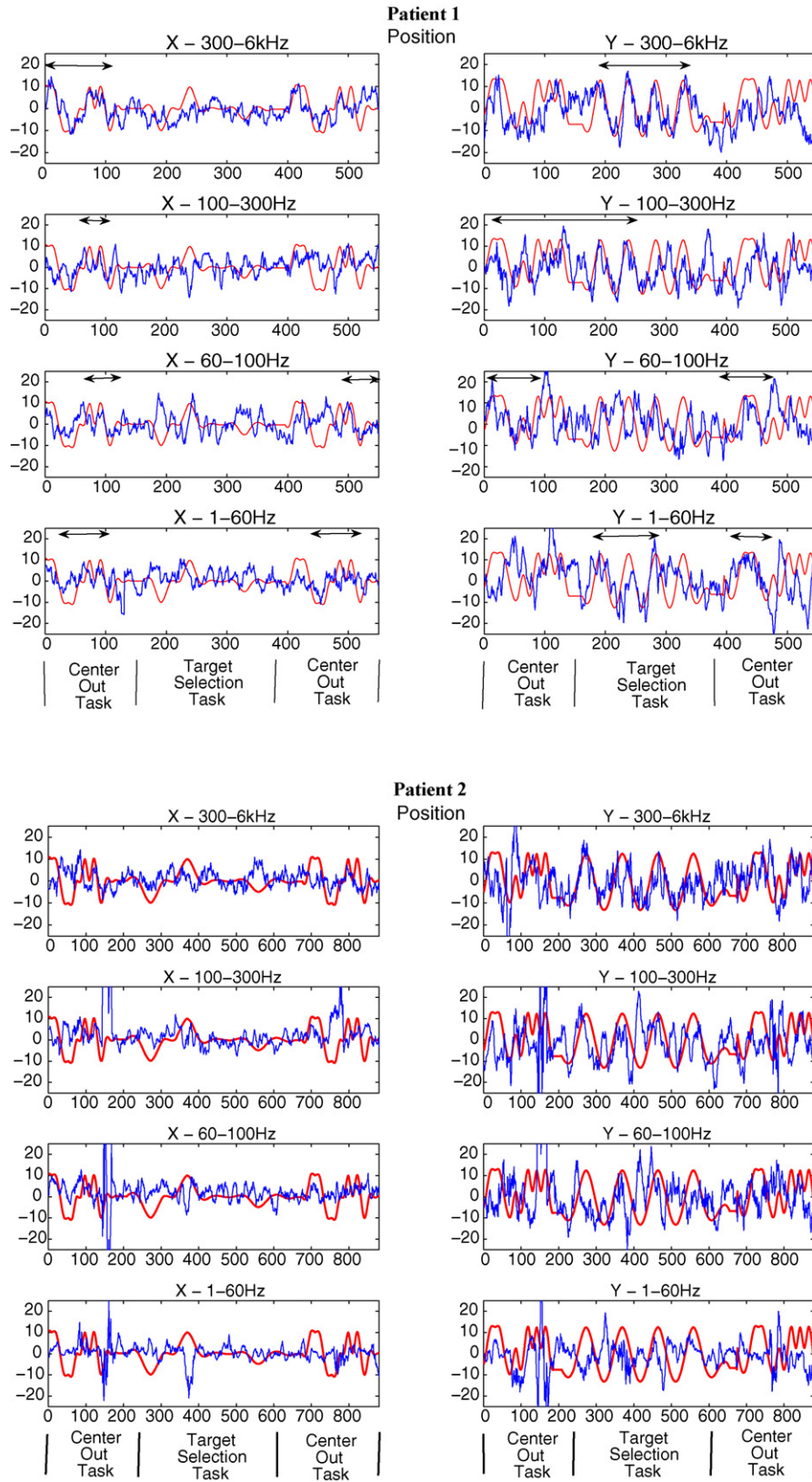


Fig. 8. Representative movement trajectories (red – actual, blue – reconstruction) over a duration of 1 min. Here, time is represented on the x-axis while displacement is on the y-axis. Note that the correlation in the trajectories varies as a function of time and frequency.

3. Results

To test the ability of the model to reconstruct the trajectory from the amplitude modulated communication and control signals extracted from the ECoG, the model weights were fixed

and novel neuronal recordings (2 min – 1200 samples) were presented. The amount of variance in the desired trajectory that was explained by the output of the model was computed using the correlation coefficient (Pearson's r) and is presented in Fig. 9 for the same segments as in Fig. 8. Here, the variation in the

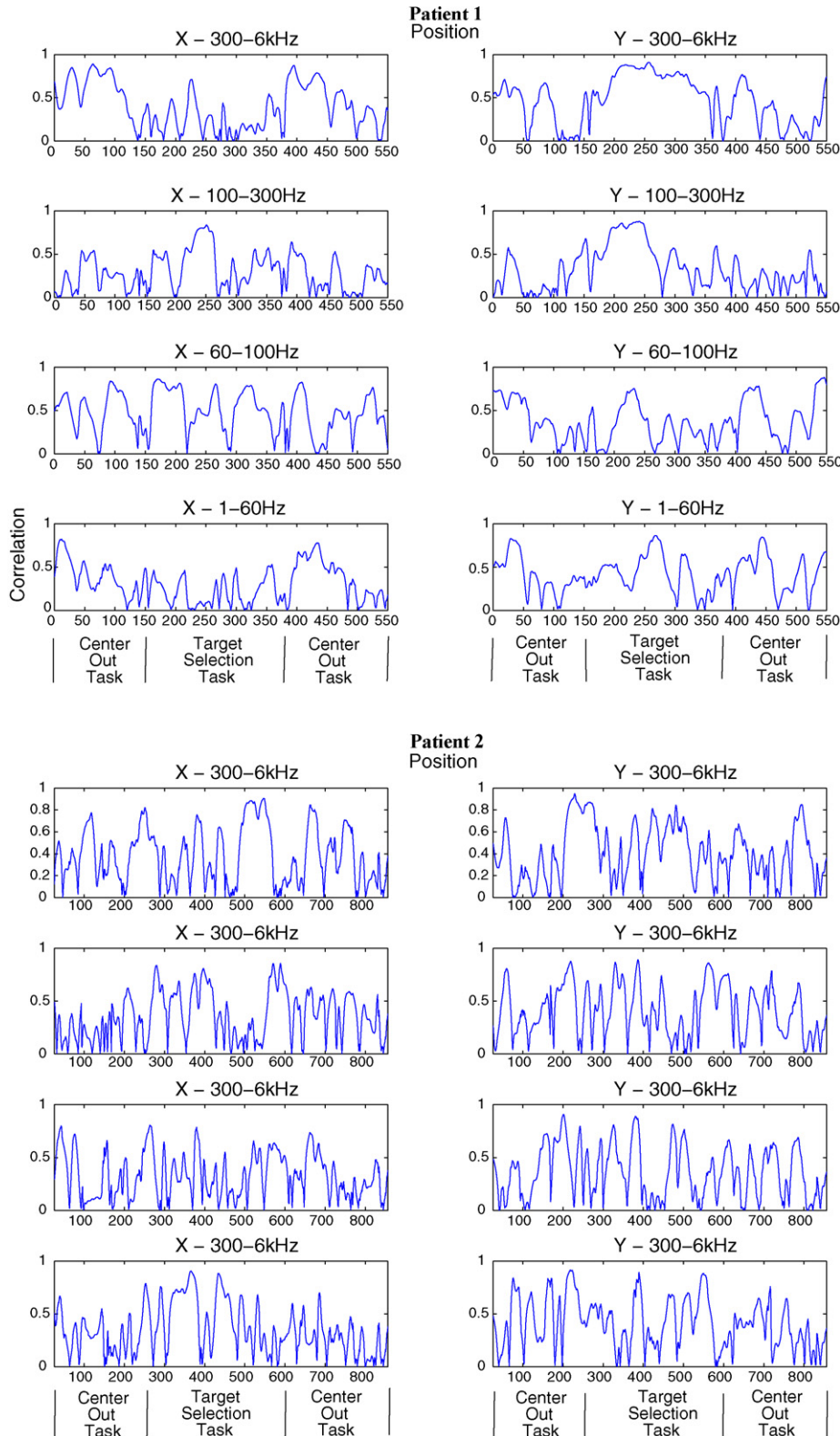


Fig. 9. Testing cross-correlation between actual hand positions and model outputs plotted over time using sliding windows.

Table 1
Correlation coefficients for broadband performance

Frequency bands	Patient 1				Patient 2			
	X-pos CC	Y-pos CC	X-pos CC ($p < 0.01$)	Y-pos CC ($p < 0.01$)	X-pos CC	Y-pos CC	X-pos CC ($p < 0.01$)	Y-pos CC ($p < 0.01$)
1–60 Hz	0.33 ± 0.16	0.41 ± 0.25	0.50	0.59	0.39 ± 0.24	0.42 ± 0.24	0.59	0.59
60–100 Hz	0.35 ± 0.24	0.41 ± 0.22	0.56	0.58	0.36 ± 0.22	0.37 ± 0.24	0.55	0.58
100–300 Hz	0.34 ± 0.21	0.35 ± 0.25	0.51	0.55	0.38 ± 0.23	0.37 ± 0.25	0.57	0.60
300–6 kHz	0.39 ± 0.26	0.48 ± 0.27	0.60	0.60	0.42 ± 0.26	0.45 ± 0.25	0.62	0.61

correlation between the model output and the desired trajectory computed using overlapping windows of 20 s (sliding in 100 ms steps) is plotted over time. The results show that there are specific instances of high correlation (above 0.90) indicating a local, task dependent nature of the data. On average for both patients, the output of the model was most correlated with the y -coordinate for all frequency bands. The trajectories produced by Patient 1 contained less variance than Patient 2 which may be due to better control with more widespread hand and arm representation as determined through microstimulation. Performance tended to increase with frequency band in the y -coordinate direction for both patients. In contrast, the x -coordinate was not predicted as well for all bands; however lower frequencies produced higher correlations for this coordinate. The correlation quantification presented here in conjunction with the representative traces presented in Fig. 8 show that continuous tracking of the hand position using amplitude modulated ECoG can be achieved. However, the trajectories are still highly variable in regions of the movement and improvements in signal processing methodologies are needed for tracking cortical and temporal performance variations.

For statistical validation and comparison with other work, we present the average correlation coefficient between the model output trajectories and the known hand positions in Table 1. To most accurately interpret the performance of the decoding in each frequency band, Fig. 9 should be compared against Table 1 to give context of temporal variation to the static values. Here, it is important to note that compared to other work in ECoG BMIs (CC ranging from 0.40 to 0.85) the correlations are computed at all points in time without any trajectory segmentation; therefore, we observe mean correlation values with significant variations. This correlation metric is focusing on the fact that each frequency band is specializing in particular temporal seg-

ments of the trajectory and may not be suitable for the entire trajectory. To determine the confidence level of the model's trajectory reconstruction in each band, we computed the significance of each windowed correlation. The mean correlation at a significance level of $p < 0.01$ is also reported which indicates that for the segments that were constructed well there is a significant relationship between the amplitude modulation regression and the hand trajectory. We note that the results presented here for natural continuous trajectories are comparable to results presented for target selection tasks of shorter duration (<5 s trials) under directional control (Leuthardt et al., 2004; Mehring et al., 2004). While there is still considerable room for improvement, this performance encourages studies for instantaneous cursor control using amplitude modulations from a broad spectrum of ECoG frequency bands. To compare the performance results with what could be expected by chance we created surrogate datasets (Prichard and Theiler, 1994) by randomizing the phase in the frequency domain of the raw ECoG recordings. The surrogate data was then bandpass filtered in the four prescribed bands and the power was computed as in Section 2.6.1. The models were retrained, tested, and the corresponding surrogate correlation coefficient values presented in Table 2 indicate that the performance of the original patient amplitude modulated data produced trajectory reconstructions above the chance level of the surrogates. We compared the correlation distributions from the surrogate models with the models trained with the original data using a two-sample Kolmogorov–Smirnov (K–S) test. In all cases, the surrogates failed the K–S test indicating with over 99% confidence that the two samples are not from the same distribution. As a second level of validation, we also computed the dependence of correlation on the highest frequency band (300–6 kHz). Since this band is the least studied in the ECoG literature, we demonstrate here the relevance of the upper cutoff

Table 2
Correlation coefficients for surrogate datasets

Frequency bands	Patient 1				Patient 2			
	X _{surr-pos} CC	Y _{surr-pos} CC	X _{surr-pos} CC ($p < 0.01$)	Y _{surr-pos} CC ($p < 0.01$)	X _{surr-pos} CC	Y _{surr-pos} CC	X _{surr-pos} CC ($p < 0.01$)	Y _{surr-pos} CC ($p < 0.01$)
1–60 Hz	^a 0.00 ± 0.23	^a 0.02 ± 0.25	0.24	0.13	^a 0.08 ± 0.38	^a 0.09 ± 0.49	0.21	0.28
60–100 Hz	^a 0.04 ± 0.35	^a 0.10 ± 0.20	0.21	0.35	^a 0.08 ± 0.35	^a 0.10 ± 0.49	0.13	0.28
100–300 Hz	^a 0.02 ± 0.29	^a 0.07 ± 0.28	0.07	0.07	^a 0.10 ± 0.37	^a 0.07 ± 0.45	0.29	0.15
300–6 kHz	^a 0.08 ± 0.32	^a 0.09 ± 0.29	0.18	0.26	^a 0.08 ± 0.43	^a 0.08 ± 0.43	0.09	0.18

^a Indicates that the surrogates failed a two-sample K-S test with $p < 0.01$

Table 3
Correlation coefficients for frequencies above 300 Hz

Frequency bands	Patient 1				Patient 2			
	X-pos CC	Y-pos CC	X-pos CC ($p < 0.01$)	Y-pos CC ($p < 0.01$)	X-pos CC	Y-pos CC	X-pos CC ($p < 0.01$)	Y-pos CC ($p < 0.01$)
300–1 kHz	0.28 ± 0.17	0.41 ± 0.21	0.52	0.58	0.35 ± 0.20	0.45 ± 0.25	0.53	0.61
300–2 kHz	0.37 ± 0.27	0.35 ± 0.25	0.62	0.59	0.41 ± 0.25	0.32 ± 0.20	0.61	0.53
300–3 kHz	0.41 ± 0.28	0.40 ± 0.24	0.61	0.57	0.32 ± 0.22	0.37 ± 0.23	0.55	0.56
300–4 kHz	0.44 ± 0.24	0.46 ± 0.23	0.61	0.59	0.40 ± 0.24	0.40 ± 0.22	0.59	0.57
300–5 kHz	0.35 ± 0.22	0.46 ± 0.27	0.55	0.65	0.34 ± 0.23	0.38 ± 0.22	0.57	0.56

limit. As in the other modeling results produced by the methods in Section 2.6.1, for Table 3 we adjusted the upper limit of the bandpass filter from 1 to 6 kHz iteratively in steps of 1 kHz. This analysis produces incremental increases in corre-

lation throughout the entire band. Increases in either the x - or y -coordinate indicate again the strong dependence of the specific frequencies for reconstruction temporal segments of the trajectory.

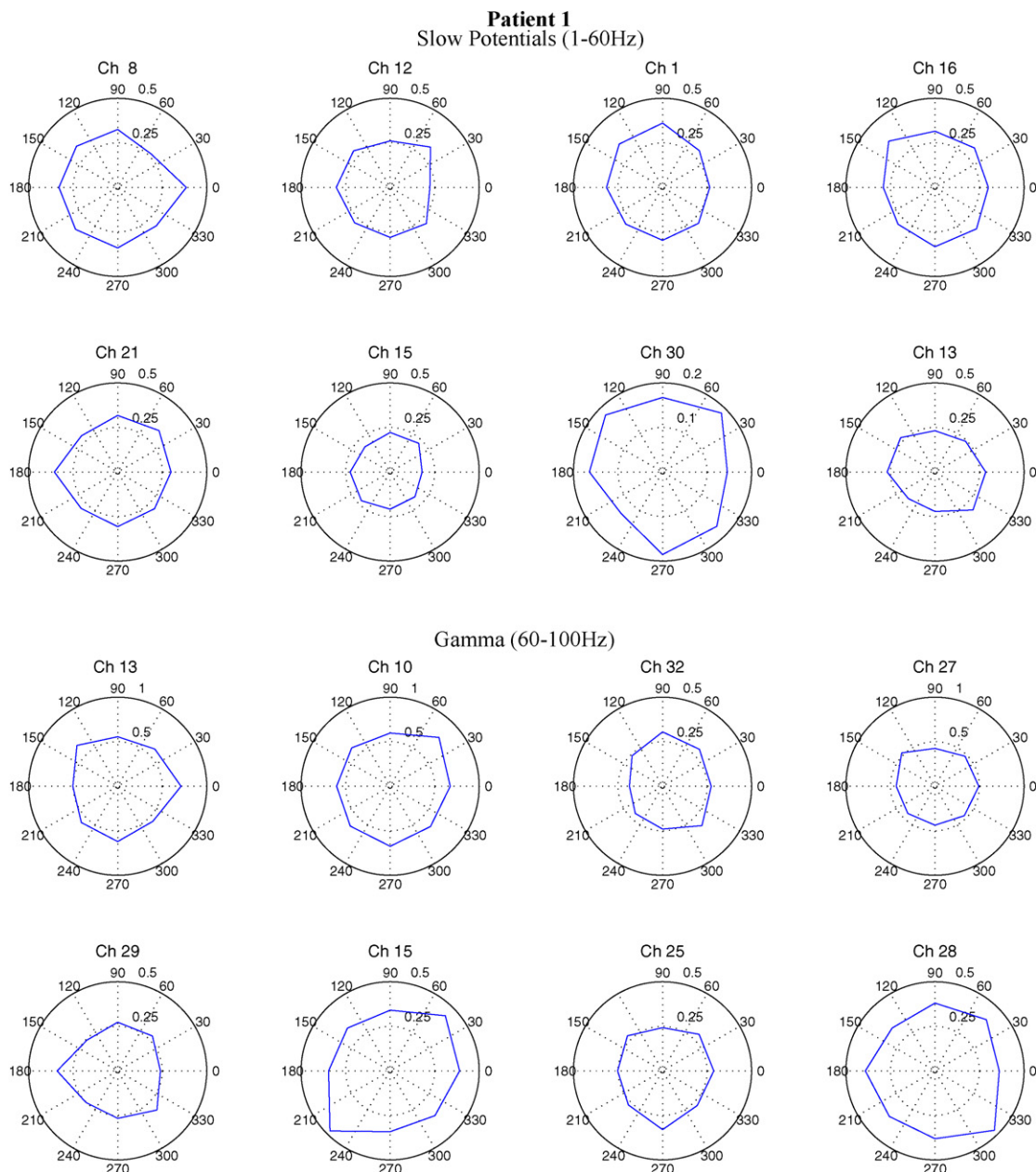


Fig. 10. Normalized tuning curves of eight electrodes that span the two dimensional hand movement space with 45° resolution in the 1–60 Hz frequency band. The coordinates of the electrodes across a 6 × 6 grid are given. (1, 1) corresponds to the left bottom corner.

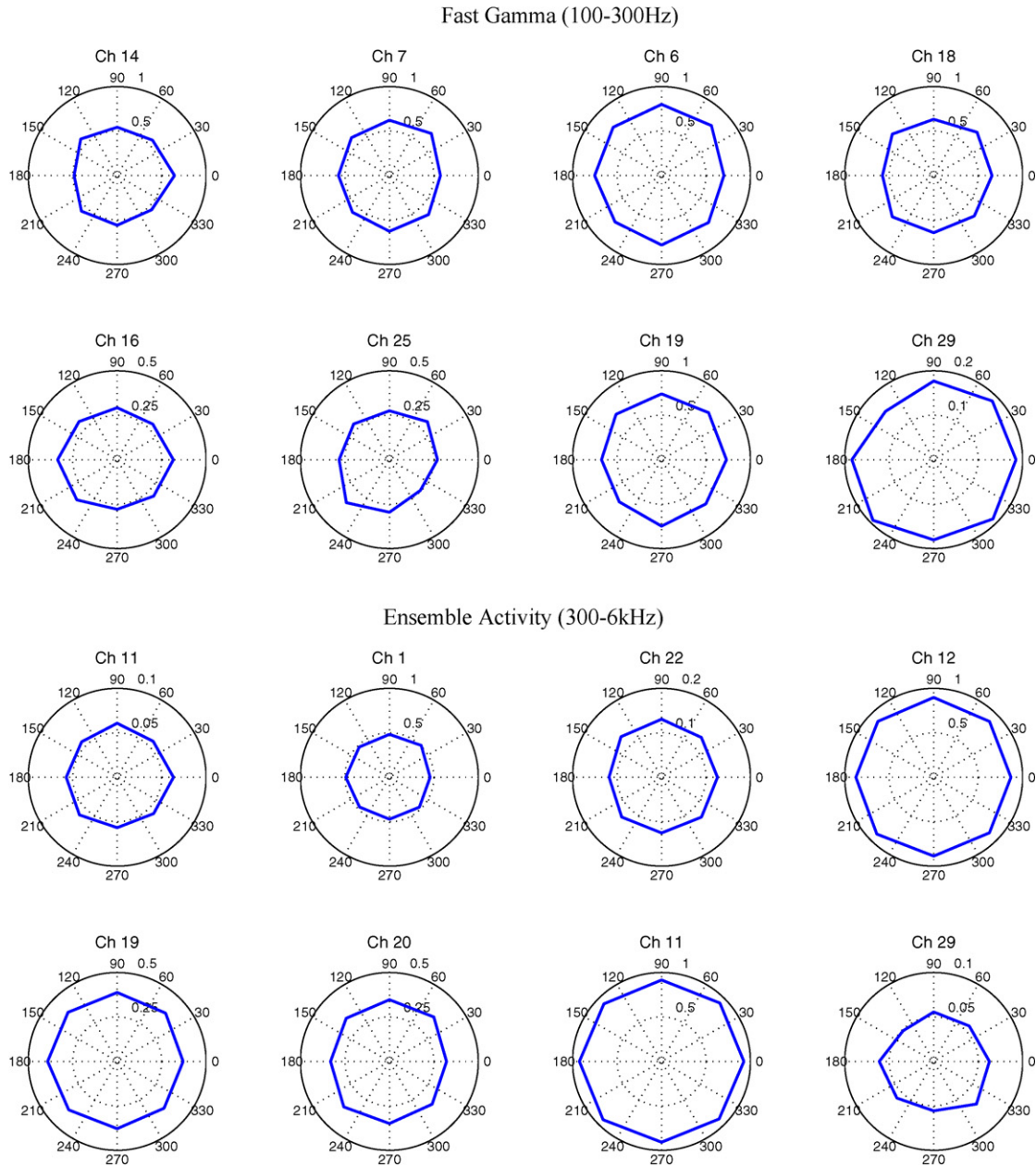


Fig. 10. (Continued).

3.1. Physiologic analysis of results

3.1.1. Directional tuning

Classically, a single motor neuron’s physiologic response to a behavioral task has been described using directional tuning curves. As originally derived from a standard center-out task by Georgopoulos et al. (1982), the tuning curve relates the mean of movement-related cell activity to movement direction. The preferred direction of a neuron, measured in degrees, is the direction which yields the maximal firing response over many trials. Weighing the preferred directions with the neural activities in the population gives a resultant direction vector called the “population vector” which has been shown to be correlated with the actual movement direction (Georgopoulos et al., 1986). Here, the directional tuning of the ECoG AM signatures are computed

(Heldman et al., 2006; Rickert et al., 2005a,b; Mehring et al., 2003a,b); however, the interpretation is potentially very different than the classical view since the ECoG is measuring an aggregate of neuronal potentials. To measure the tuning performance of the ECoG AM signatures, the *Tuning depth* will be defined as the difference between maximum and minimum tuning over the hand movement space for a channel (greater depths imply better performance).

Herein, we analyze the tuning of the AM ECoG recordings to the hand movement direction in the selected frequency bands. The space of hand movement direction ranging from 0° to 360° was divided into 8 bins with 45° of resolution. Initial tuning analysis indicated an interference amongst neighboring channels or interference from a common noise source due to common peaks in the tuning curves. Compared to adaptive filtering, tun-

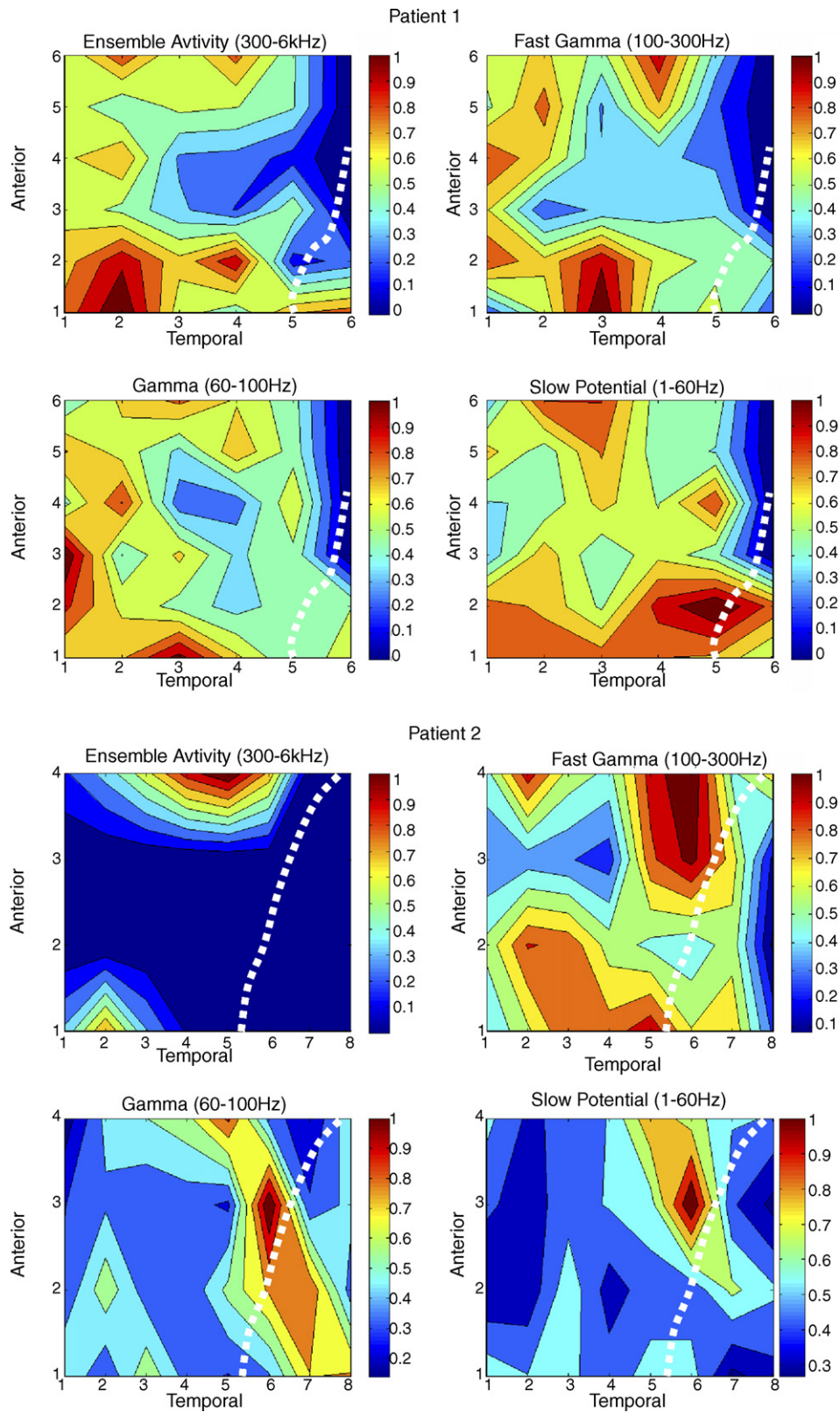


Fig. 11. Tuning depth of electrodes as a function of physical placement and frequency bands. The dotted white line indicates the location of the central sulcus as determined using MRI.

ing analysis does not have the ability to minimize the effects of noise. This problem was overcome by spatially filtering the electrode recordings with Laplacian filters, which subtract a quarter of the four neighborhoods of an electrode recording from itself (Gonzalez and Woods, 2002). This suppresses the common trend in neighboring electrodes and emphasizes the individual features of an electrode. After spatial filtering, the two-dimensional hand direction space is spanned for each frequency band, i.e. at least one electrode is tuned to the center of each 45° bin. Fig. 10 shows representative tuning curves for Patient 1 in the four frequency bands that span the whole space. The tuning curves were normalized by the standard deviation of the power across the channels for spatial comparison and the calculated tuning depths are presented in Fig. 11 across the different frequency bands for the two patients studied here. To provide context to the images, we have superimposed the position of the central sulcus as determined through analysis of the MR images (Mehring et al., 2004). For Patient 1, the highest tuning depth in the primary motor area that was mapped with electrical stimulation is evident in the highest two frequency bands. This may be attributed to the trend that high frequency signals are more localized. On the other hand, for the slowest frequency band, in which synchronous activity is widespread in larger areas of the cortex, tuned electrodes are spread all across premotor, somatosensory and primary motor cortices. In the gamma band, which has been associated with cognitive temporal binding (Makeig, 1993; Engel and Singer, 2001), well-tuned electrodes are mainly localized in the premotor area. For Patient 2, the electrodes to which the patient responded to stimulation with her hand (electrodes 2, 3) are highly tuned in the highest two frequency bands, whereas electrodes that caused arm response (electrodes 14, 15) are highly tuned in the slow frequency, gamma, and fast gamma bands. The most widely spread tuned electrodes across the motor cortex are evident in the fast gamma band.

While directional tuning provides a useful physiologic interpretation, it is subject to two issues when applied to ECoG. The higher level of abstraction of ECoG signals compared to action and local field potentials previously discussed introduces a confound of specificity when using tuning for ECoG. Limited spatial resolution and broad frequency range make decoding of motor information from ECoG recordings a challenging problem. Since ECoG recordings can be considered as cumulative sums of neural activity across a population, they yield broader tuning curves as seen in Fig. 11 compared to those of sharply tuned single-unit activities reported in the literature. This phenomena was also encountered by Mehring (Mehring et al., 2004) who showed that the P1, P2, N1, N2 features of LFPs were absent in movement onset averaged ECoG signals. Second, tuning curves may change as a function of the delay used to align neural activity with the execution of the movement. An optimal delay time should yield higher tuning depths and would be in the range of physiological reaction times of the movement. If the neural activity is delayed more than an acceptable reaction time, the preferred direction of the tuning may change as an artifact of inaccurate time alignment between the activity and hand movement. In our simulations, we observed changes in the preferred direction across channels and frequency bands when

the neural activity was delayed by more than 200 ms. Plotting tuning depths as a function of delay time demonstrated peaks around 100 ms for the majority of the channels and thus this was chosen as the time duration we shift the neural activity for alignment with the hand movement. (For 10 Hz sampling frequency this corresponds to a one sample shift).

3.1.2. Sensitivity analysis applied to ECoG

Theoretical analysis of the spatio-temporal activation of coordinated neural ensembles has attempted to define the regions of interest involved in cortical processing however they are subject to the problems described in Section 3.1.1. Here, we derive the activation directly from the model and experimental ECoG data as a function of the analyzed frequency band. A sensitivity analysis (Sanchez et al., 2003a,b) can be performed by computing the Jacobian of the output vector with respect to each neuronal input i as shown in (4). For a well trained model, this calculation also indicates which inputs are most important for modulating the desired trajectory of the model. Hence, an electrode's importance can be determined by simply reading the corresponding weight value in the trained model, if the input data for every channel is power normalized. Since for ECoG data this is not the case, the electrode importance is estimated in the vector Wiener filter by multiplying the absolute value of an electrode's sensitivity with the standard deviation of its amplitude computed over the dataset as in (5). To obtain a scalar sensitivity value for each electrode, the weight values are also averaged over the twenty-five delays and output dimensions.

$$\frac{\partial \mathbf{y}_j}{\partial \mathbf{x}_i} = \mathbf{W}_{25(i-1)+1:25(i-1)+25,j} \quad (4)$$

$$s_i = \sigma_i \frac{1}{2} \sum_{j=1}^2 \frac{1}{25} \sum_{k=1}^{25} |\mathbf{W}_{10(i-1)+k,j}| \quad (5)$$

In Fig. 12, the normalized sensitivity contours are presented and spatially arranged to match the electrode grids in Fig. 2A and B. Again, to provide context to the images, we have superimposed the position of the central sulcus as determined through analysis of the MR images (Mehring et al., 2004). Several trends can be observed here. First, we see that for both patients the bands and the electrodes that best reconstructed the hand trajectory were highly localized in the primary motor and somatosensory cortices with less activation in the premotor cortex. Both the gamma and high-gamma oscillations produced similar activation localized in the premotor cortex. For Patient 1 the gamma activity was more strongly and diffusely represented in the premotor cortex than Patient 2. The slow potentials produced diffuse activation broadly across the primary motor cortex in Patient 1 with smaller activation in premotor while in Patient 2 the sensitive electrodes were primarily located in premotor and to a lesser extent in primary motor cortex.

Comparing Figs. 11 and 12 we observe that there is overlap of the peaks of Wiener filter sensitivity and tuning depth in cortical areas over the same frequency ranges however the sensitivity analysis provides more discrete localization. For Patient 1, the most distinct localization is evident for the highest frequency

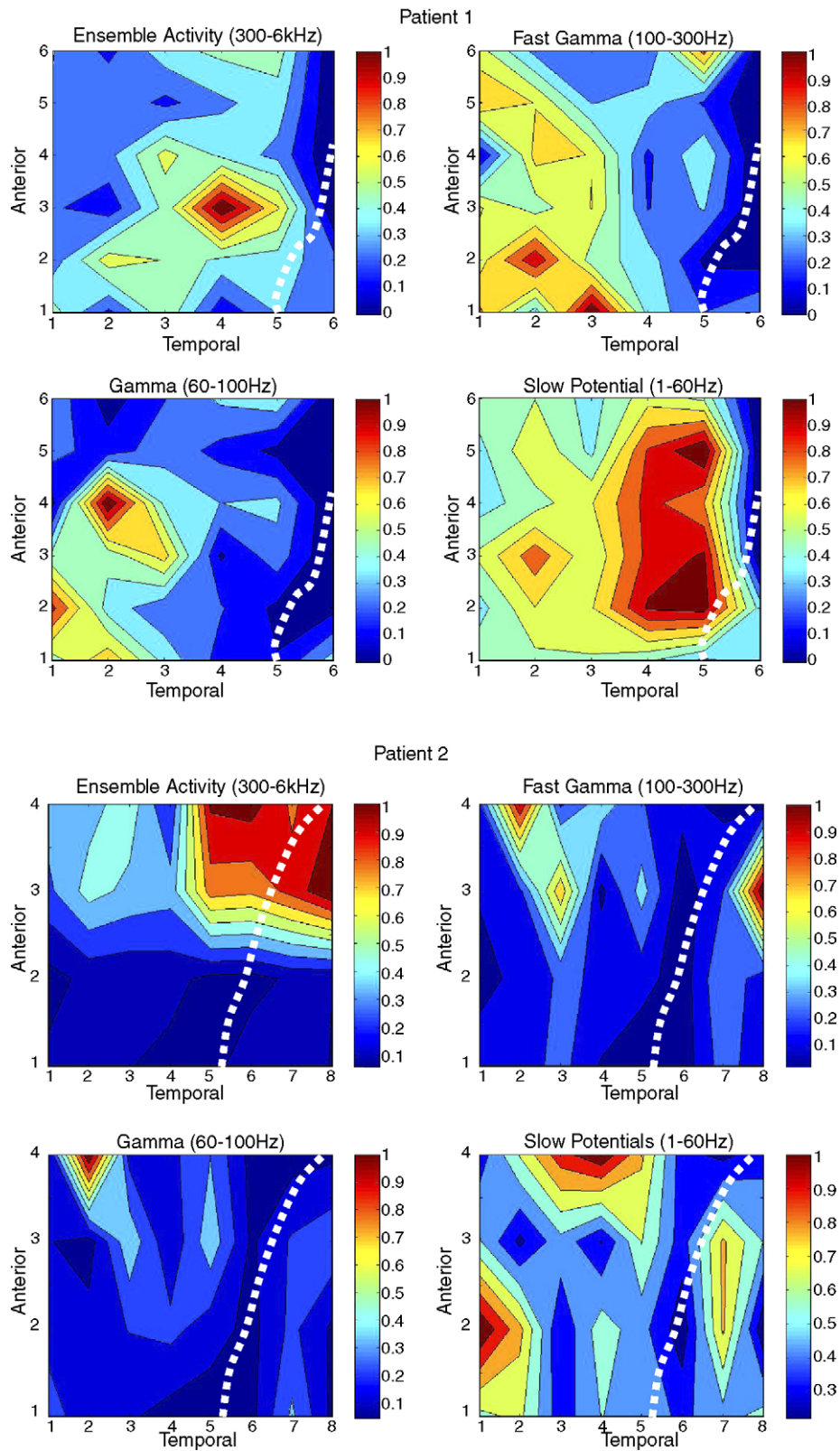


Fig. 12. Regions of maximal sensitivity for each band. Significant channels in the gamma and fast gamma bands cluster in the premotor cortex while electrodes in the ensemble and slow bands are in the primary motor cortex. The dotted white line indicates the location of the central sulcus as determined using MRI.

range. For the most sensitive electrode in the Wiener analysis in this band, we observed that the largest Wiener coefficients were for the taps far into the past. This history is not reflected into the tuning analysis and hence the sensitivity of that electrode is not reflected into a high tuning depth. In the case of Patient 2 and the gamma band, the two analysis techniques provided results that are complementary. Wiener sensitivity analysis emphasizes the importance of the electrodes to which the patient yielded a hand response, whereas tuning analysis demonstrates high tuning for the electrodes to which the patient yielded arm response.

4. Discussion

The neuroprosthetic testing design presented here indicates how synergistic development of signal processing tools with experimental recording in clinical environments can open new possibilities for the advancement of rehabilitative neural interfaces. In the clinical setting, the needs of the recording hardware for diagnosis do not necessarily coincide with the needs to expand the spectra of extracted control signals. Clinical based neurophysiological methods for analyzing neuromodulation also takes advantage of human interaction and instructed behavior to elicit neural activation. Such interaction between subject and algorithm development is difficult to achieve in animal paradigms involving operant conditioning. Human-based closed-loop control studies will likely provide the necessary motor control task complexity and feedback to assess control features and quantify adaptation of neuromodulation in dynamically changing neurorehabilitation environments.

By overcoming the limitations of human clinical ECoG recordings we have taken advantage of the neural ensemble (300 Hz to 6 kHz) activity which provides decoding opportunities that may form the basis for human ECoG neuroprostheses. The advancement was made possible through the use of custom amplification and DSP neural recording hardware. While the external hardware to the patient plays a strong role in the ability to extract spatially localized and temporally intermittent control signatures, the scale of the subdural electrodes internal to the patient also play a role in the ability to resolve control commands. Therefore, one should be cautious of the choice of electrode technology used in ECoG recording. A systematic and simultaneous evaluation of ECoG electrode scales is required in the future.

Defining continuously varying feature vectors from ECoG for deriving communication and control commands is a significant challenge in neuroprosthetic design. Building upon rate coding theory and observations from visual, auditory, and motor ERD studies, this analysis indicated that the computation of “rate-like” amplitude modulations provides a viable control parameter for producing neural interfaces capable of therapeutic performance. We would like to present a note of caution here that unlike rate codes in microelectrode recordings which can be specific to a single neuron, the amplitude modulations in ECoG can be influenced by neuromodulation not related to movement. For example, in the epileptic patients studied here, interictal spikes could potentially bias the amplitude modulation. There-

fore, improvements in techniques for decoupling the relevant neuromodulation from noise is of critical importance.

In terms of sensorimotor rhythms, all frequency bands within slow, gamma, fast-gamma, and ensemble activation bands produce some contribution to the task indicating a mixture of experts modeling approach using all frequency bands may also improve performance. Since each frequency band produces spatially distinct activation, one approach to neuroprosthetic design may be to tailor the extraction of the potentials to the patient using the signal processing techniques described here. The linking of theoretical analysis of mesoscopic neuronal activation with data driven signal processing techniques has provided a rich interpretation of the underlying physiology and provided insight for the next steps in neuroprosthetic development.

While the performance of the trajectory reconstruction provides an indication that we have selected a viable control parameter, the spatial activation of the amplitude modulations reveal the different cortical organization during movement at different frequency bands. Our working hypothesis is that they are a novel window to understand cortical organization during movement in the absence of more specific brain theories, and they are very useful to also implement neuroprosthetics. The shortcomings are several and need to be improved: (1) The model assumes stationarity so there is a lack of temporal resolution in these plots; (2) the models are trained with mean square error so it is only capturing second order statistics of the relationships between brain signals and movement; (3) the sensitivity is only totally reliable for accurate models (i.e. when the modeling error is small); (4) the number of patients in this study is small (i.e. this limits our ability to generalize the understanding of cortical organization). Nevertheless, methodology presented here provides a framework which others can apply to many other types of behavioral studies to try to elucidate generalizations about neural function.

Here, we have presented a technique based on amplitude modulation in spontaneous ECoG activity for instantaneous cursor control using an optimal signal processing perspective. However, as shown in this study, the trajectory reconstructions often have large variances due to the inability to control in real-time the contributions of electrodes containing neuronal modulation not related to the task. Therefore, the ability to identify and separate spontaneous spatio-temporal distinct activity from noise in real-time is critical to the success of such an approach. This study as well as others (Mehring et al., 2004; Leuthardt et al., 2003) is seeking to overcome these challenges to show the great potential for patients to use multiresolution neural activity to generate natural movements which could be directly translated into cursor control. In our next experiments, we seek to optimally select ECoG electrodes that produce the most information for the trajectory reconstruction while finding a projection that decorrelates the noisy channels.

Acknowledgements

This work was supported in part by The Children’s Miracle Network and the B.J. and Eve Wilder Epilepsy Research Endowment. The authors would like to thank David Smullen

M.D., Assistant Professor of Neuroradiology, at the University of Florida for his help in the MRI grid localization. The authors are also grateful for the assistance of the Shands Hospital Epilepsy Monitoring Unit team.

References

- Abeles M. Local cortical circuits. New York: Springer-Verlag; 1982.
- Aertsen A, Hauske G, Tsukada M. Special issue on dynamic brain. *Biol Cybernet* 2003;88:319–20.
- Andersen RA, Musallam S, Pesaran B. Selecting the signals for a brain–machine interface. *Curr Opin Neurobiol* 2004;14:720.
- Barrie JM, Freeman WJ, Lenhart M. Modulation by discriminative training of spatial patterns of gamma EEG amplitude and phase in neocortex of rabbits. *J Neurophysiol* 1996;76:520–39.
- Desmurget M, Pelisson D, Rossetti Y, Prablanc C. From eye to hand: planning goal-directed movements. *Neurosci Biobehav Rev* 1998;22:761.
- Editorial. Is this the bionic man? *Nature* 2006;442:p. 109.
- Engel AK, Singer W. Temporal binding and the neural correlates of sensory awareness. *Trends Cogn Sci* 2001;5:16–25.
- Engel AK, Moll CKE, Fried I, Ojemann GA. Invasive recordings from the human brain: clinical insights and beyond. *Nat Rev Neurosci* 2005;6:35–47.
- Freeman WJ. Mass action in the nervous system: examination of the neurophysiological basis of adaptive behavior through EEG. New York: Academic Press; 1975.
- Freeman WJ. Mesoscopic neurodynamics: from neuron to brain. *J Physiol (Paris)* 2000;12/1;94:303–22.
- Freeman WJ. Origin, structure, and role of background EEG activity. Part 1. Analytic phase. *Clin Neurophysiol* 2004a;115:2077–88.
- Freeman WJ. Origin, structure, and role of background EEG activity. Part 2. Analytic amplitude. *Clin Neurophysiol* 2004b;115:2089–107.
- Freeman WJ. Origin, structure, and role of background EEG activity. Part 3. Neural frame classification. *Clin Neurophysiol* 2005;16:1118–29.
- Freeman WJ. Origin, structure, and role of background EEG activity. Part 4. Neural frame simulation. *Clin Neurophysiol* 2006;117:572–89.
- Freeman WJ, van Dijk B. Spatial patterns of visual cortical fast EEG during conditioned reflex in a rhesus monkey. *Brain Res* 1987;422:267–76.
- Georgopoulos A, Kalaska J, Caminiti R, Massey J. On the relations between the direction of two-dimensional arm movements and cell discharge in primate motor cortex. *J Neurosci* 1982;2:1527–37.
- Georgopoulos AP, Schwartz AB, Kettner RE. Neuronal population coding of movement direction. *Science* 1986;233:1416–9.
- Gonzalez RC, Woods RE. Digital image processing. New Jersey: Prentice Hall; 2002.
- Haykin S. Adaptive filter theory. 3rd ed. Upper Saddle River, NJ: Prentice-Hall International; 1996.
- Heldman DA, Wang W, Chan SS, Moran DW. Local field potential spectral tuning in motor cortex during reaching. *IEEE Trans Neural Syst Rehabil Eng* 2006;14:180–3.
- Jasper H, Penfield W. Epilepsy and the functional anatomy of the human brain. Boston: Little, Brown and Co; 1954.
- Johnson RN, Quint SR, Brickley JJ, Charlton JD, Lee SI, Hanna GR. Evoked-potentials as indicators of brain dynamics—results from an interactive computer system. *Ann Neurol* 1977;1:500–1.
- Lesser RP, Gordon B, Fisher RS, Vining E, Uematsu S. Cortical stimulation using subdural electrodes. *J Epilepsy* 1990;3:103–6.
- Leuthardt EC, Schalk G, Wolpaw JR, Gilliam F, Ojemann J, Moran D. Developing a brain–computer interface utilizing subdural electrodes in seizure-monitored patients. *Neurosurgery* 2003;53:475–6.
- Leuthardt EC, Schalk G, Wolpaw JR, Ojemann JG, Moran DW. A brain–computer interface using electrocorticographic signals in humans. *J Neural Eng* 2004;1:63–71.
- Leuthardt EC, Schalk G, Moran D, Ojemann JG. The emerging world of motor neuroprosthetics: a neurosurgical perspective. *Neurosurgery* 2006;59:1–13.
- Lutzenberger W, Birbaumer N, Flor H, Rockstroh B, Elbert T. Dimensional analysis of the human EEG and intelligence. *Neurosci Lett* 1992;143:10–4.
- Makeig S. Gamma-band event-related brain dynamics—historic perspective. *Int J Psychophysiol* 1993;14:136–136.
- McFarland DJ, Lefkowitz AT, Wolpaw JR. Design and operation of an EEG-based brain–computer interface with digital signal processing technology. *Behav Res Methods Instrum Comput* 1997;29a:337–45.
- Mehring C, Rickert J, Vaadia E, Cardoso de Oliveria S, Aertsen A, Rotter S. Inference of hand movements from local field potentials in monkey motor cortex. *Nat Neurosci* 2003a;6:1253–4.
- Mehring C, Rickert J, Vaadia E, de Oliveira SC, Aertsen A, Rotter S. Inference of hand movements from local field potentials in monkey motor cortex. *Nat Neurosci* 2003b;6:1253–4.
- Mehring C, Nawrot MP, Cardoso de Oliveira S, Vaadia E, Schulze-Bonhage A, Aertsen A, et al. Comparing information about arm movement direction in single channels of local and epicortical field potentials from monkey and human motor cortex. *J Physiol (Paris)* 2004;98:498–506.
- Nicolelis MAL. Methods for neural ensemble recordings. Boca Raton: CRC Press; 1999.
- Nunez PL. Electric fields of the brain: the neurophysics of EEG. New York: Oxford University Press; 1981.
- Nunez PL. Generation of human EEG by a combination of long and short range neocortical interactions. *Brain Topogr* 1989;1:199–215.
- Nunez PL. Neocortical dynamics and human EEG rhythms. New York: Oxford University Press; 1995.
- Pfurtscheller G, da Silva FHL. Event-related EEG/MEG synchronization and desynchronization: basic principles. *Clin Neurophysiol* 1999;110:1842–57.
- Pfurtscheller G, Graimann B, Huggins JE, Levine SP, Schuh LA. Spatiotemporal patterns of beta desynchronization and gamma synchronization in corticographic data during self-paced movement. *Clin Neurophysiol* 2003;114:1226.
- Prichard D, Theiler J. Generating surrogate data for time series with several simultaneously measured variables. *Phys Rev Lett* 1994;73.
- Rickert J, Cardoso de Oliveira S, Vaadia E, Aertsen A, Rotter S, Mehring C. Encoding of movement direction in different frequency ranges of motor cortical local field potentials. *J Neurosci* 2005a;25:8815–24.
- Rickert J, de Oliveira SC, Vaadia E, Aertsen A, Rotter S, Mehring C. Encoding of movement direction in different frequency ranges of motor cortical local field potentials. *J Neurosci* 2005b;25:8815–24.
- Riehle A, Grun S, Diesmann M, Aertsen A. Spike synchronization and rate modulation differently involved in motor cortical function. *Science* 1997;278:1950–3.
- Sanchez JC, Kim SP, Erdogmus D, Rao YN, Principe JC, Wessberg J, et al. Input-output mapping performance of linear and nonlinear models for estimating hand trajectories from cortical neuronal firing patterns. In: In International Work on Neural Networks for Signal Processing; 2002. p. 139–48.
- Sanchez JC, Carmena JM, Lebedev MA, Nicolelis MAL, Harris JG, Principe JC. Ascertaining the importance of neurons to develop better brain machine interfaces. *IEEE Trans Biomed Eng* 2003a;61:943–53.
- Sanchez JC, Erdogmus D, Rao YN, Principe JC, Nicolelis MAL, Wessberg J. Learning the contributions of the motor, premotor, and posterior parietal cortices for hand trajectory reconstruction in a brain machine interface. In: In IEEE EMBS Neural Engineering Conference; 2003b. p. 59–62.
- Sanchez JC, Carney PR, Principe JC. Analysis of amplitude modulated control features for ECoG neuroprosthetics. In: In IEEE International Conference of the Engineering in Medicine and Biology Society; 2006.
- Schalk G, McFarland DJ, Hinterberger T, Birbaumer N, Wolpaw JR. BCI2000: A general-purpose, brain–computer interface (BCI) system. *IEEE Trans Biomed Eng* 2004;51:1034–43.
- Scott SH. Neuroscience: converting thoughts into action. *Nature* 2006;442:141.
- Serruya MD, Hatsopoulos NG, Paninski L, Fellows MR, Donoghue JP. Brain-machine interface: instant neural control of a movement signal. *Nature* 2002;416:141–2.
- Shadmehr R, Wise SP. The computational neurobiology of reaching and pointing: a foundation for motor learning. Cambridge, MA: The MIT Press; 2005.
- Sinai A, Bowers CW, Crainiceanu CM, Boatman D, Gordon B, Lesser RP, et al. Electrocorticographic high gamma activity versus electrical cortical stimulation mapping of naming. *Brain* 2005;128:1556–70.

- Taylor DM, Tillery SIH, Schwartz AB. Direct cortical control of 3D neuroprosthetic devices. *Science* 2002;296:1829–32.
- Thatcher RW, Krause PJ, Hrybyk M. Cortico-cortical associations and EEG coherence: a two-compartmental model. *Electroencephalogr Clin Neurophysiol* 1986;64:123–43.
- Vaughan TM, Wolpaw JR. The third international meeting on brain–computer interface technology: making a difference. *IEEE Trans Neural Syst Rehabil Eng* 2006;14:126–7.
- Wennekers T, Sommer F, Aertsen A. Editorial: cell assemblies. *Theory Biosci* 2003;122:1.
- Wessberg J, Stambaugh CR, Kralik JD, Beck PD, Laubach M, Chapin JK, et al. Real-time prediction of hand trajectory by ensembles of cortical neurons in primates. *Nature* 2000;408:361–5.
- Wise SP, di Pellegrino G, Boussaoud D. The premotor cortex and nonstandard sensorimotor mapping. *Can J Physiol Pharmacol* 1996;74:469–82.
- Wolpaw JR, Birbaumer N, McFarland DJ, Pfurscheller G, Vaughan TM. Brain–computer interfaces for communication and control. *Clin Neurophysiol* 2002;113:767–91.
- Worrell GA, Cranstoun SD, Echaz J, Litt B. Evidence for self-organized criticality in human epileptic hippocampus. *Neuroreport* 2002;13:2017–21.